# Fused Deposition Modeling and microwave sintering of 3Y-TZP samples

Clémence Petit, Christophe Meunier, Lucas Manceaux, Hugo Rivera, Hubert Taxil

# Fused Deposition Modeling and microwave sintering of 3Y-TZP samples

Clémence Petit*, Christophe Meunier, Lucas Manceaux, Hugo Rivera, Hubert Taxil

Mines Saint-Etienne, Univ Lyon, CNRS, UMR 5307 LGF, F-42023 Saint-Etienne France

*Corresponding author: Clémence Petit, clemence.petit@emse.fr

**Abstract**

Fully dense zirconia parts were produced by shaping using Fused Deposition Modeling (FDM) and microwave (MW) sintering. The samples were obtained using an usual 3D printer and a commercial 3 mol% yttria-stabilized zirconia filament. The printing parameters were adapted to the printer and the filament. Then, the samples were debinded with a two-step process, *i.e.*, chemical and thermal debinding. The debinded samples were sintered in a multimode microwave instrumented cavity. Full density was achieved with shorter thermal cycles compared with conventional sintering. Dilatometric curves for microwave sintering show similar behavior during densification, as in conventional sintering. The evolution of measured temperature vs time confirms the good control of the thermal cycle allowed by the MW device.

**Keywords:** Zirconia, Additive Manufacturing, Microwave sintering

## 1. Introduction

Fused Deposition Modeling (FDM) is a material extrusion process which is commonly used to print polymer-based objects [1]. FDM uses a thermoplastic polymeric filament which is heated and extruded from a nozzle through two rollers. The object to be printed is governed by various material and machine parameters, as layer resolution, build orientation, or extruder temperature, [2]. The Computer-Aided Designed model of the object to print is sliced by a slicer. The G-Code obtained from the slicer is an input for the nozzle to move in the XY plane until a single

layer is completed. Then, the building platform moves in the Z direction and the process is repeated until all the layers have been printed.

FDM can also be applied to fabricate ceramic or metallic parts from specific filaments made of polymeric binders and a ceramic or metallic powder. During the last years, parts made of various ceramics as alumina [3,4] or zirconia [5,6] were produced by FDM. Compared to other additive processes, FDM has the advantages of high flexibility, low cost and easiness of use. But, despite these advantages, the ceramic parts made by FDM still have to undergo long thermal cycles to remove the binders and sinter them. These post-processing stages can prevent the development of additive manufacturing (AM) and particularly FDM for a large-scale production. For this reason, the development of rapid sintering processes has a particular interest to be coupled with shaping by AM. Among them, microwave (MW) sintering has the advantages of being pressureless (unlike *e.g.*, SPS). Some authors show the possibility to sinter large pieces with a homogeneous heating by a careful control of the setup (especially the choice of susceptors) [7]. Moreover, MW sintering has already been applied to sinter different ceramics and especially zirconia [8, 9]. Few authors tried to sinter by MW ceramic objects shaped by stereolithography [10, 11] or robocasting [12]. Up to now, no study deals with MW sintering of ceramics shaped by FDM.

The aim of this study is to produce zirconia parts by combining FDM with a commercial filament used in a desktop printer and MW sintering. Different parts were produced and their density was measured. Dilatometric curves and MW powers were recorded and compared to conventional (CV) sintering process.

## 2. Experimental procedures

The samples were prepared from a commercial 3 mol% yttria-stabilized zirconia (3Y-TZP) filament (*Zetamix White Zirconia, Nanoe, France*). This filament was made from 50 vol% 3Y-TZP powder and 50 vol% organic binders (the detailed composition is confidential).

Different pellets were printed with a commercial desktop 3D printer (*3D Volumic Stream 30 Dual*), equipped with a nozzle with a diameter of 0.6 mm. The following printing parameters were determined by different preliminary tests: layer height of 0.15 mm, extrusion temperature of 200°C, layer width of 0.6 mm, printing speed of 25 mm/s. The samples were printed with an infill density of 100% and a rectilinear pattern. The slicer was PrusaSlicer®.

A two-step debinding stage was chosen according to the supplier's requirement. First, for the chemical debinding samples were placed in an acetone bath. To minimize the occurrence of cracks, we optimized this step by monitoring the mass loss during debinding. Different durations in the acetone bath were tested. The samples were weighed before and after staying in acetone. The optimum time obtained for this chemical step was 4 hours at 40°C where the mass loss was about 7% (no additional mass loss for duration higher than 4 hours). Then, they were thermally debinded at 8°C/h to 500°C in an electric furnace (*Thermolyne 6000*).

The samples were sintered in a CV furnace (*Naberthem*) and a MW cavity with the following thermal cycles: temperature of 1475°C, dwell time of 30 min and heating rates of 25°C/min for CV sintering and 25, 50 and 80°C/min for MW sintering.

MW sintering was carried out in a multimode cavity, connected with a magnetron powered by a 3 kW generator working at a frequency of 2.45 GHz (*GMP30K, SAIREM, France*). More information can be found in [13, 14]. The green samples were positioned in a sintering cell to guarantee a thermal insulation and a homogeneous heating. This cell has been described in [10]. It was made of different plates of aluminosilicate fibers (*KVS 184-400, Rath®, Germany*) and a SiC susceptor. The cavity was instrumented with a pyrometer and a camera to control the

thermal cycle, measure the temperature and follow the shrinkage by optical dilatometry. A bichromatic infrared pyrometer (*Lumasense Technology, Germany*), sensitive to wavelengths between 2 and 2.5 μm and working in the 250–1800 ◦C temperature range was used for temperature measurement. The pyrometer allowed a contactless measurement of temperature (pyrometer outside the cavity). The ratio of emissivity was set to 1. A PID feedback loop was used to control the incident power required to achieve the targeted heating rate. A Labview interface (*National Instruments, USA*) recorded the temperatures and microwave powers. The shrinkage of the pellets was followed with optical dilatometry, which is a contactless shrinkage measurement [14]. During the thermal cycle, images of the flat surface of the pellets were recorded and then used to detect the pellets' edges with a Labview software.

The density of the sintered samples was measured thanks to Archimedes' method (theoretical density of 6.07 g/cm$^3$ for 3Y-TZP). The samples were observed with an optical microscope (*Olympus GX51*).

## 3. Results and discussion

Table 1 presents the values of the relative densities of the sintered pellets. The MW-sintered pellets reached a high level of densification, similar to the one for CV sintering, whatever the heating rate. In particular, it can be noted that the shortest thermal cycle (*i.e.*, heating rate of 80°C/min) achieved comparable values, in comparison with the longer ones.

Figure 1 shows the dilatometric curves of the different sintered pellets. MW and CV sintering achieved the same level of linear shrinkage (Figure 1a). Small differences (temperature of onset of densification, linear shrinkage reached in the intermediate stage of sintering) are visible between the curves for MW sintering (Figure 1b). They are probably related to difficulties to estimate the linear shrinkages with optical dilatometry (based on image analysis of the samples

during heating, so disturbed by their own thermal irradiation). Differences in behavior of the samples during sintering is less probable.

Figure 2 shows an image from optical microscopy showing a residual pore between layers. Despite the infill density of 100%, some residual open spaces were observed after sintering and are probably created during printing. Some authors have already observed this type of defects for ceramics printed by FDM [15]. It explains the values of relative densities lower than 99%. An optimization of the printing path during slicing would be beneficial to obtain fully dense pieces.

*Table 1: Relative densities of the sintered samples*

| Samples | Relative density (% TD) |
|---|---|
| MW – 25°C/min | 93.9 |
| MW – 50°C/min | 97.7 |
| MW – 80°C/min | 96.8 |
| CV – 25°C/min | 96.8 |

Figure 3a shows the evolution of the MW powers and the measured temperature during a MW thermal cycle and Figure 3b focuses on the 600-1200°C range. The measured temperature correctly followed the set one, evidencing the possibility to control the heating cycle. From the room temperature to ~ 800°C, the incident MW power increases to follow the set temperature. At ~ 800°C, a small disturbance zone is visible in the heating step. Around this temperature, a small decrease of incident and absorbed power followed by a plateau is visible. Then, from 1000 to 1400°C, the absorbed power increases and the reflected power stays constant. This evolution of MW power can be related to the evolution of dielectric properties of 3Y-TZP, *i.e.*, dielectric loss of 3Y-TZP is known to increase from 500°C [16]. A higher level of MW power is certainly absorbed by the sample to be heated.

## 4. Conclusion

MW sintering has been used to densify zirconia pellets shaped by FDM with a commercial filament and a desktop printer. It resulted in highly dense samples with shorter thermal cycles in comparison with CV sintering (*i.e.*, 80°C/min vs 25°C/min). The MW and CV dilatometric curves show similar behaviour during densification. The temperature vs time curve during MW sintering shows a quite good control of thermal cycle. However, some residual pores probably created during the printing process were observed. It shows the need to optimize the printing strategy to print fully dense samples. It opens the way to the possibility of a rapid production of ceramic parts for prototyping or small series production, by associating additive manufacturing and MW sintering. In particular, some materials, like 3Y-TZP, are particularly interesting for this because of its high coupling capability with MW.

## 5. References

[1] V. Dhinakaran, K.P. Manoj Kumar, P.M. Bupathi Ram, M. Ravichandran, M. Vinayagamoorthy, Mater. Today: Proc. 27 (2020) 752-756.

[2] S. Khan, K. Joshi, S. Deshmukh, Mater. Today Proc. 50 (2022) 2119-2127.

[3] S. Mamatha, P. Biswas, P. Ramavath, D. Das, R. Johnson, Ceram. Int. 44 (2018) 19278-19281.

[4] M. Orlovská, Z. Chlup, Ľ. Bača, M. Janek, M. Kitzmantel, J. Eur. Ceram. Soc. 40 (2020) 4837-4843.

[5] D. Nötzel, R. Eickhoff, C. Pfeifer, T. Hanemann, Materials 14 (2021) 5467.

[6] A. Hadian, L. Koch, P. Koberg, F. Sarraf, A. Liersch, T. Sebastian, F. Clemens, Add. Manuf. 47 (2021) 102227.

[7] S. Marinel, C. Manière, A. Bilot, C Bilot, C. Harnois,G. Riquet, F. Valdivieso, C. Meunier, C. Coureau, F. Barthélemy, Materials 12 (2019) 2544.

[8] C. Monaco, F. Prete, C. Leonelli, L. Esposito, A. Tucci, Ceram. Int. 41 (2015) 1255-1261.

[9] Á. Presenda, M.D. Salvador, F.L. Peñaranda-Foix, R. Moreno, A. Borrell, Ceram. Int. 41 (2015) 7125-7132.

[10] N. Khalile, C. Meunier, C. Petit, F. Valdivieso, B. Coppola, P. Palmero, Ceram. Int. 49 (2023) 7350-7358.

[11] H. Curto, A. Thuault, F. Jean, M. Violier, V. Dupont, J.-C. Hornez, A. Leriche, J. Eur. Ceram. Soc. 40 (2020) 2548-2554.

[12] J. Ravoor, R. E. Selvam, Ceram. Int. 49 (2023) 12585-12595.

[13] J. Chassagne, C. Petit, C. Meunier, F. Valdivieso, Mater. Today Comm. 33 (2022) 104679.

[14] D. Zymełka, S. Saunier, J. Molimard, D. Goeuriot, Adv. Eng. Mater. 13 (2011) 901-905.

[15] M. Orlovská, M. Hain, M. Kitzmantel, P. Veteška, Z. Hajdúchová, M. Janek, M. Vozárová, Ľ. Bača, Add. Manuf. 48 (2021) 102395.

[16] M. Arai, J.G.P. Binner, T.E. Cross, J. Microwave Power Electromagnetic Energy 31 (1996) 12-18.

**Figures' captions**

Figure 1: Linear shrinkage of (a) the MW and CV-sintered samples and (b) the MW-sintered samples with different heating rates

Figure 2: Image from optical microscopy of the MW-25°C/min sintered sample, showing residual pores due to printing

Figure 3: (a) Evolution of temperature and MW incident, absorbed and reflected powers during a MW thermal cycle and (b) magnified view on the temperature range 600-1200°C

Fig 1:

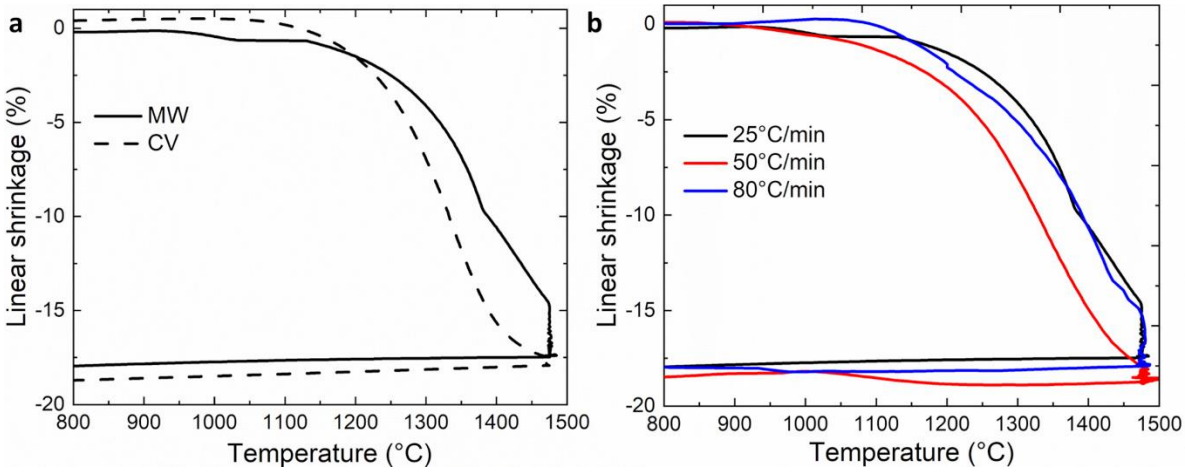
a
b
Linear shrinkage (%)
Temperature (°C)
MW
CV
25°C/min
50°C/min
80°C/min
0
-5
-10
-15
-20
800
900
1000
1100
1200
1300
1400
1500

Fig 2:

Fig 3:

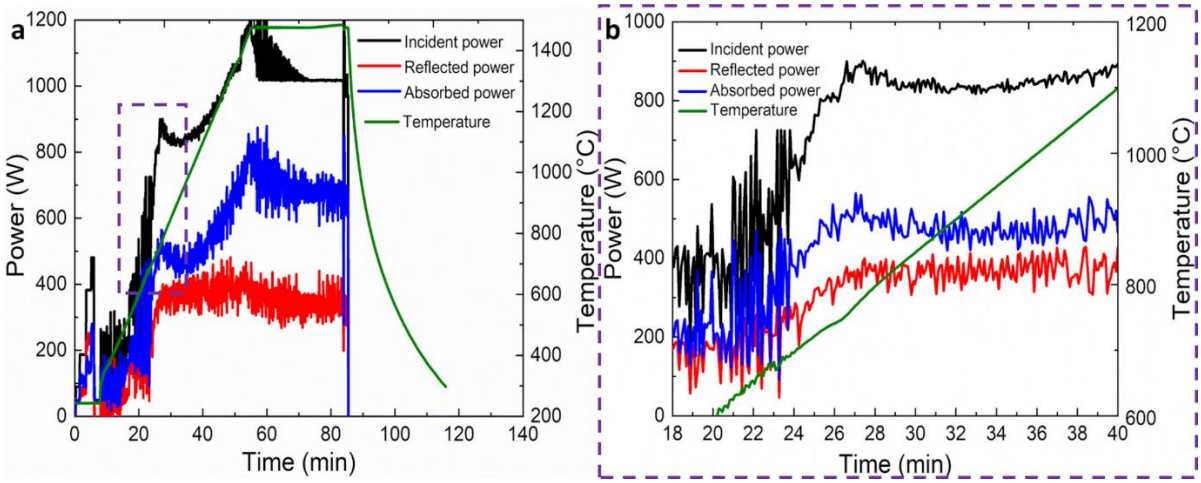
a
b
Incident power
Reflected power
Absorbed power
Temperature
Power (W)
Temperature (°C)
Time (min)